Mechanochemical Metathesis between $AgNO_3$ and NaX (X = Cl, Br, or I), and Ag_2XNO_3 Double Salt Formation

Stipe Lukin,[†] Tomislav Stolar,[†] Ivor Lončarić,[†] Igor Milanović,[‡] Nikola Biliškov,[†] Marco di Michiel,[¶] Tomislav Friščić,[§] and Ivan Halasz*,[†]

†*Ruđer Bošković Institute, Bijenička 54, 10000 Zagreb, Croatia*

‡*Department of Physics (010), Vinča Institute of Nuclear Sciences - National Institute of the Republic of Serbia, University of Belgrade, Mike Petrovića Alasa 12-14, 11000, Belgrade, Serbia*

¶*ESRF - the European Synchrotron, 71 Avenue des Martyrs, 38000 Grenoble, France*

§*Department of Chemistry, McGill University, 801 Sherbrooke St. W., H3A 0B8 Montreal, Canada*

E-mail: ivan.halasz@irb.hr

Abstract

Here we describe real-time, *in situ* monitoring of mechanochemical solid-state metathesis between silver nitrate and the entire series of sodium halides, based on tandem powder X-ray diffraction and Raman spectroscopy monitoring. The mechanistic monitoring reveals that reactions of $AgNO_3$ with NaX (X = Cl, Br, I) differ in reaction paths, with only the reaction with NaBr providing the $NaNO_3$ and AgX products directly. Reaction with NaI revealed the presence of a novel, short-lived intermediate phase, while the reaction with NaCl progressed the slowest and through the well-defined Ag_2ClNO_3

intermediate double salt. While the corresponding iodide and bromide double salts were not observed as intermediates, all three are readily prepared as pure compounds by milling equimolar mixtures of AgX and $AgNO_3$. The *in situ* observation of reactive intermediates in this simple metathesis reactions reveals a surprising resemblance of reactions involving purely ionic components to those of molecular organic solids and cocrystals. This study demonstrates the potential of *in situ* reaction monitoring for mechanochemical reactions of ionic compounds, as well as completes application of these techniques to all major compound classes.

Introduction

Mechanochemistry, *i.e.* chemical reactions performed by exerting mechanical force on solid reactants, has become recognised as a viable synthetic route and an alternative to solution-based protocols.[1–6] Applied to organic,[7–10] inorganic,[11–14] organometallic,[15–19] coordination and supramolecular chemistry,[20–23] as well as to the preparation of nanoparticles,[14,24] metal-organic frameworks,[25–29] main group compounds[30–33] and catalysis,[34–40] mechanochemical reactions are most often performed in closed containers, or vessels, that oscillate, rotate, or swing.[24,25] In such conditions, obtaining information about the reaction course was attainable only by periodically interrupting the milling process for sampling of the reaction mixture.[41–48] However, with each reaction vessel opening, the conditions inside the milling vessel are disrupted and the reaction mixture experiences hardly reproducible temperature variations,[49] as well as exposure to atmospheric gases and moisture. Also, if the mechanochemically-induced reaction continues to proceed after cessation of milling,[50–53] subsequent analysis of such samples, will not accurately represent the chemical and physical changes during milling.

It is therefore, no surprise that the recent development of *in situ* techniques for uninterrupted reaction monitoring has been a breakthrough in the study and understanding of milling processes and dynamics.[54] These methods, based on powder X-ray diffraction (PXRD),[55–58] Raman spectroscopy,[59–63] temperature[49,64] and pressure monitoring,[65? –67] and

their simultaneous application,[49,68–71] revealed complex milling reaction mechanisms,[72] involving new polymorphic phases,[68,73] as well as multi-step mechanisms,[74–77] with crystalline and amorphous intermediates.[54,76,78]

So far, *in situ* monitoring was applied to reactions of almost all classes of compounds, with the notable exception of reactions of inorganic ionic compounds.[11,12,79–81] Here, we provide the first *in situ* and real-time investigation of a purely inorganic mechanochemical transformation, targeting an ion metathesis reaction that is highly familiar to most chemists when conducted in solution: immediate formation of an insoluble silver halide upon mixing aqueous solutions of $AgNO_3$ and a sodium halide NaX (X = Cl, Br or I). In aqueous solution, this prototypical reaction is often used as a qualitative test for halide ions since it is dominated by the extremely low solubility of silver halides AgCl, AgBr and AgI. Solubility however, should not have a role if this reaction would be conducted in the absence of water or another solvent, prompting the herein presented ball milling solid-state processes. Based on standard Gibbs energies of formation of reactants and target products, reactions of $AgNO_3$ and sodium halides, except for NaF, are thermodynamically favourable and as such should be feasible also in the solid state (Figure 1).

Mixtures of solid reactants in the 1:1 molar ratio were milled using a vibratory ball mill to yield the expected products, $NaNO_3$ and AgX (X = Cl, Br or I), which was evidenced by PXRD. Reaction paths and rates however, varied through the series of sodium halides. While the reaction with NaCl was the slowest, and that with NaI the fastest overall, only milling with NaBr yielded the products directly from reactants. We also demonstrate that milling is efficient for preparation of mixed salts Ag_2ClNO_3, Ag_2BrNO_3, and Ag_2INO_3. Among these double salts, only Ag_2ClNO_3 was observed to form as an intermediate during milling of $AgNO_3$ and NaX.

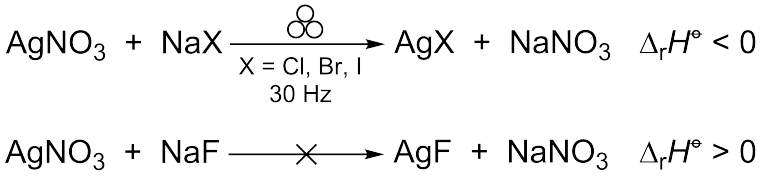

Figure 1: Reactions of silver(I) nitrate and sodium halides.

Experimental section

Solution precipitation of AgCl, AgBr, and AgI. 5 mmol of $AgNO_3$ and NaX were dissolved separately in 20 mL of re-distilled water and slowly mixed while ensuring minimal exposure to light. The precipitate formed immediately upon mixing, it was filtered, washed with water and dried in air for 3 h followed by drying in a desiccator under reduced pressure of argon for three days in the dark.

Laboratory powder X-ray diffraction (PXRD) patterns were collected on an Aeris Panalytical diffractometer using Ni-filtered copper radiation in the Bragg-Brentano geometry with the sample prepared in a thin layer on a silicon zero-background holder.

Reaction monitoring. In situ real-time reaction monitoring was achieved by tandem PXRD and Raman spectroscopy *in situ* at the ID15A beamline of the ESRF - The European Synchrotron in Grenoble, as previously described,[68] using a remotely-controlled IST500 (In-Solido Technologies, Croatia) mixer mill operating at 30 Hz. The X-ray beam ($E = 70$ keV, $\lambda = 0.1771$ nm) was set to pass through the bottom of a poly(methyl methacrylate (PMMA) reaction vessel. Exposure time was set to 4 s and a waiting time was added to match the 5 second interval between consecutive frames. Diffraction data were collected on a Dectris Pilatus3 X CdTe 2M detector positioned 730 mm from the sample. We performed radial integration of the raw diffraction images with an ESRF in-house MATLAB script. Raman spectroscopy employs a portable Raman system with a PD-LD (now Necsel) BlueBox laser source having an excitation wavelength of 785 nm and an OceanOptics (now OceanInsight) Maya2000Pro spectrometer coupled with a B&W-Tek fiber optic BAC102 probe. The position of the probe was about 0.8 cm from the bottom of the vessel. Raman spectra were

collected every 10 s with an acquisition time of 500 ms and summing 20 scans for each spectrum.

As milling vessels, 14 mL PMMA vessels with two 5 mm tungsten carbide (WC) balls (each weighing 1.4 g) were used. Reactants were milled in the 1 : 1 stoichiometric ratio, and we have kept the total mass of the reaction mixture to 250 mg, adjusting the masses of reactants with different molecular weights. During weighing, vessels were wrapped with aluminum foil to minimize its exposure to light, and which was removed after mounting the vessel onto the ball mill. Light was switched off in the experimental hutch during milling, and the sample may have experienced only minimal exposure to light, except for the Raman laser beam. The ambient temperature in the experimental hutch was 21 °C. Experiments were typically reproduced three times.

Quantitative Rietveld analysis was performed in an automated fashion in the command-line version of the program Topas usually starting from the same input file for each diffraction pattern. Parameters that were refined included coefficients of the shifted Chebyshev polynomial for background description, and parameters describing peaks shape and size: Lorentzian and Gaussian full widths at half maximum, zero shift and unit cell parameters. Crystal structure models for reactants and products were checked against the Inorganic Crystal Structure Database (ICSD) or the Crystallography Open Database (COD). Atomic coordinates of the structure models were not refined. For $AgNO_3$ the ICSD entry 1685 was used. For NaCl the ICSD entry 18189 and for NaBr the ICSD entry 26910. Crystal structure models of $NaNO_3$ polymorphs were taken from the ICSD entry 2865 for the ordered polymorph and from the ICSD entry 180920 for the disordered one. For AgCl, AgBr and AgI, ICSD entries 64734, 65061 and 56552, respectively, were used.

Analysis of Raman spectra was performed in MATLAB using in-house scripts. Raman spectra were truncated to the region $1100 - 765\,\mathrm{cm}^{-1}$ and were baseline-corrected using the asymmetric least-squares (ALS) algorithm.[82] Data were normalized by dividing all spectrum data points with the intensity of the peak at $812\,\mathrm{cm}^{-1}$, which belongs to the PMMA reaction

vessel. For fitting intensities of Raman peaks at 1046 and 1070 cm^{-1}, we selected the 1085 − 1025 cm^{-1} spectral range (Figure S2) that was fitted using two Gaussian functions of the general form:

$$f(x) = Ae^{-[(x-x_0)/c]^2} + O$$

where A is band intensity, x_0 is peak position, c is band width, and O is linear offset.

The density functional theory calculations were performed with a plane-wave basis set code VASP.[83,84] We used PBE exchange-correlation functional,[85] with the energy cutoff set to 520 eV. The core-electron interaction was approximated by projector augmented wave (PAW) potentials.[86] The Brillouin zone was sampled with a Monkhorst-Pack mesh[87] with a density of at least 4 Å. The structures were optimized until change in the energy was smaller than 0.0005 eV.

Residual Gas Analysis (RGA). The composition of gaseous products was conducted by a home-made RGA device with MKS Vac-Check LM78 quadrupole mass spectrometer. We introduced the gaseous products of mechanochemical reaction in RGA apparatus by putting the stainless steel capillary (internal diameter of 0.15 mm and length of 1 m) in the milling vessel. The total pressure of high vacuum (HV) system was 2.5×10^{-6} mbar during the measurements. Analysis of the atmosphere inside the vessel, by measuring the partial pressures, was conducted by following the m/z ratios of 28 (for N_2), 30 (NO), 32 (O_2), 46 (NO_2), 70 ($^{35}Cl_2$), 76 (N_2O_3), and 92 (N_2O_4).

Results and discussion

A consideration of thermodynamic data (Table S1) indicates that all reactions of $AgNO_3$ and NaX, except the one involving NaF, are thermodynamically favourable and should proceed at standard conditions (Table 1). Standard reaction enthalpies and standard Gibbs energies of reaction for NaX (X = Cl, Br, or I) are negative, while the standard reaction enthalpy for

the reaction with NaF is positive. Since entropy contribution to Gibbs energy of ionic solids at room temperature is generally small compared to enthalpy, it can be safely assumed that in the case of NaF, standard Gibbs energy of reaction should also be positive. As expected, PXRD analysis of the milled $AgNO_3$ and NaF mixture revealed no new products, even after two hours of milling (Figure S1). As the reaction mixture remained a physical mixture of reactants it was not considered for an *in situ* study.

Table 1: Standard reaction enthalpies and Gibbs energies for a general reaction NaX + $AgNO_3 \longrightarrow NaNO_3 + AgX$ (X = Cl, Br, or I).[88]

X	$\Delta_r H^{\ominus}$/kJ mol^{-1}	$\Delta_r G^{\ominus}$/kJ mol^{-1}
F	28.5	
Cl	−59.3	−59.4
Br	−82.8	−81.5
I	−117.5	−113.7

$AgNO_3$ + NaCl

In a first set of *in situ* experiments we milled $AgNO_3$ and NaCl. Aside from the formation of AgCl and $NaNO_3$, *in situ* PXRD data revealed the appearance of an intermediate phase (Figure 2a), which was identified as Ag_2ClNO_3, based on PXRD analysis. This phase was previously prepared from an aqueous mixture of $AgNO_3$ and AgCl at 90 °C, and from the melt.[89] Attempting Rietveld analysis of the *in situ* collected PXRD patterns using the crystal structure of $NaNO_3$ in the $R\bar{3}c$ space group could not provide satisfactory refinements of all PXRD patterns. This problem was resolved upon recognizing that $NaNO_3$ had crystallized in a mixture with its other polymorph, having the $R\bar{3}m$ space group.[90] By including both polymorphs, we were able to obtain satisfactory Rietveld refinements for patterns collected through the entire milling experiment. The crystal structure of the polymorph crystallizing in the $R\bar{3}c$ space group (herein designated $NaNO_3$-c), is ordered and stable at room temperature, while the polymorph having the $R\bar{3}m$ space group (designated $NaNO_3$-m) is the high-temperature polymorph exhibiting disorder of the nitrate anion.[90]

The Inorganic Crystal Structure Database (FIZ Karlsruhe) lists around 40 entries for the two polymorphs of $NaNO_3$ and the phase transition between the two polymorphs has been the subject of numerous studies.[91–93] It is described to be of the second order with the disorder of the nitrate becoming more and more pronounced as the temperature increases up to 550 K when the two positions of the nitrate anion become equally populated, the c axis is halved and the space group is changed from $R\bar{3}c$ to $R\bar{3}m$. In our case, the *in situ* formation of the $R\bar{3}m$ high-temperature polymorph can be considered as surprising as these temperatures are never reached on the bulk of the sample during ball milling on a vibratory mill. Its formation may tentatively be attributed to kinetic factors and understood as being in accordance with the Ostwald's rule of stages.[94,95]

Formation of the expected products AgCl and $NaNO_3$ commenced almost immediately after the onset of milling (Figure 2b). After about two minutes, we witnessed appearance of Ag_2ClNO_3, which continued crystallizing simultaneously with $NaNO_3$-c, $NaNO_3$-m, and AgCl for the next 20 min. At that time, Ag_2ClNO_3 and $NaNO_3$-m started to slowly deplete until, after $\sim$ 60 min of milling, only AgCl and $NaNO_3$-c were detectable in the reaction mixture. The reaction profile for the formation of AgCl seems to exhibit two different regimes (Figure 2b). After initial growth in the first 10 min, the formation of AgCl started to follow a sigmoidal trend, indicating a change in mechanism of crystal growth of AgCl product. At the early stages of the reaction, $AgNO_3$ was the principal source of Ag^+ ions for the formation of both AgCl and Ag_2ClNO_3. As the reaction proceeded and the amount of $AgNO_3$ depleted, the formation of Ag_2ClNO_3 slowed down and the latter eventually became the source of Ag^+ ions for the growth of AgCl. Consequently, the formation of AgCl is the result of more than one chemical reaction. This is further evident from significantly different rates of depletion of NaCl and $AgNO_3$, as Ag_2ClNO_3 is also the source of Cl^- ions in the formation of AgCl.

Noteworthy, Rietveld analysis yielded an unrealistically high total weight fraction for $NaNO_3$ throughout the middle part of the reaction. We rationalize the higher then expected

weight fraction of $NaNO_3$ by recognising that the nascent AgCl may be partially amorphous. The final weight fractions of 62.7 % and 37.3 % for AgCl and $NaNO_3$, respectively, are close to the theoretically expected values based on the starting equimolar mixture of $AgNO_3$ and NaCl. A partially amorphous reaction mixture, even for ionic compounds, may not be surprising as AgCl may form as a partially amorphous material upon fast precipitation from solution,[96] and milling is a long-used approach not only for comminution and reduction of particle sizes, but also an effective way of amorphization of organic, metal-organic, and inorganic materials.[97–101] *In situ* Raman spectroscopy monitoring in this experiment was of no use due to strong fluorescence which completely saturated the detector, even at a very low laser power.

$AgNO_3 + NaBr$

In our second set of *in situ* experiments, we explored the milling reaction of $AgNO_3$ and NaBr. Here, we observed a direct steady transformation from reactants to AgBr and $NaNO_3$ without any intermediate (Figure 3a). According to Rietveld refinement, the transformation was complete within 10 min of milling (Figure 3b). The formation of AgBr and $NaNO_3$ exhibited an first-order kinetics trend, much the same as was observed for AgCl in the first 10 min. Such similar kinetics could indicate the same reaction mechanism of double ion-exchange between $AgNO_3$ and NaCl or NaBr at the onset of milling and before a significant amount of the intermediate Ag_2ClNO_3 has been formed. Here again, after 10 min of milling, there was a steady drop of the weight fraction of $NaNO_3$ from 32 to 30 %, which can also be contributed to crystallization of AgBr that may have initially formed in a partially amorphous state. Final weight fractions for $NaNO_3$ and AgBr are in good agreement with their theoretical values of 32 % and 68 %, respectively (Figure 3b).

Unlike the reaction involving NaCl, the reaction of $AgNO_3$ and NaBr exhibited significantly lower fluorescence in Raman spectra. Nevertheless, we observed a broad fluorescence signal in the spectral region from 1800 to 3250 cm^{-1} (Figure S3). As the reaction proceeded,

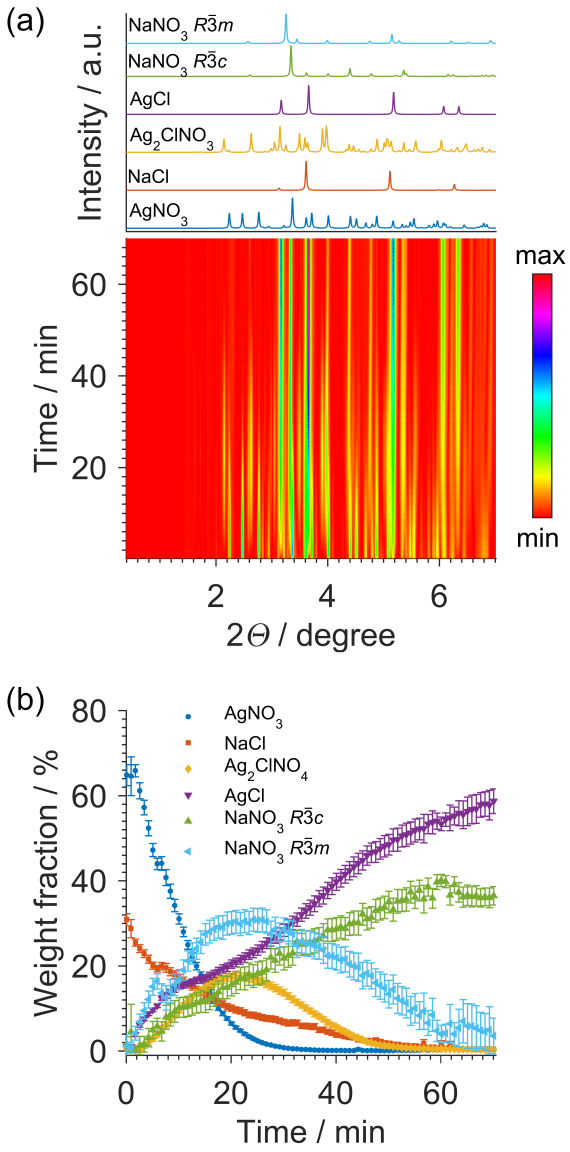

Figure 2: Milling of $AgNO_3$ and NaCl. (a) *in situ* reaction monitoring by synchrotron PXRD. Diffraction patterns of reactants and products are given above the 2D time-resolved spectra. (b) Weight fractions derived from the Rietveld refinement of the above diffraction patterns.

the fluorescence gradually diminished, correlating with the loss of the intensity of the Raman band at 1046 cm^{-1} and the appearance of a new band at 1070 cm^{-1} (Figure 3c). Both these bands correspond to symmetric stretching of the NO_3^- ion, the band at 1046 cm^{-1} to NO_3^- stretching in $AgNO_3$, and the band at 1070 cm^{-1} to NO_3^- stretching in $NaNO_3$.[102,103] Intensities of these bands can be used to obtain a reaction profile that displays depletion of $AgNO_3$ and formation of $NaNO_3$ (Figure 3d). Although intensities of Raman peaks are proportional to amounts of $AgNO_3$ and $NaNO_3$, careful calibration would still be needed for exact quantification. Despite this, curves in both, PXRD and Raman monitoring derived reaction profiles, exhibit similar trends. While weight fractions of $NaNO_3$ have dropped steadily from 32 to 30 % (Figure 3b) after 10 min of milling, intensities of of the $NaNO_3$ Raman band remained constant (Figure 3d). Again, we find a likely explanation of these observations in crystallization of partially amorphous nascent AgBr, which would then lower the weight fraction of $NaNO_3$, even if its amount and crystallinity remains steady.

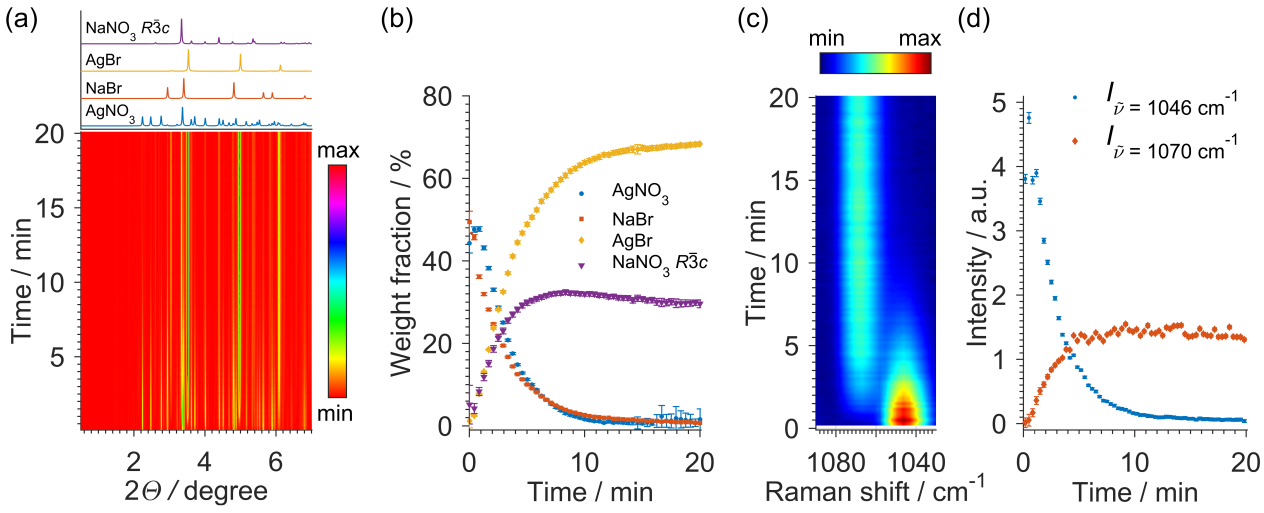

Figure 3: Milling of $AgNO_3$ and NaBr. (a) *In situ* reaction monitoring by synchrotron PXRD. Diffraction patterns of reactants and products are given above the 2D time-resolved spectra. (b) Weight fractions derived from the Rietveld refinement of the *in situ* PXRD patterns. (c) 2D time-resolved Raman spectra for the Raman spectral range $1088 - 1030\,cm^{-1}$. (d) The change of Raman peak intensities at 1046 and 1070 cm^{-1} during milling.

$AgNO_3 + NaI$

Before presenting results of milling of $AgNO_3$ and NaI, we note that NaI that we had used contained a small amount of one or more of unidentified impurities (Figure S5), which could have affected reactivity of NaI, and these observations should be considered with caution. Milling $AgNO_3$ and NaI resulted in a fast reaction that was complete within 13 min, according to PXRD and Raman spectroscopy (Figure 4). To our surprise, the PXRD data revealed a remarkable transient intermediate phase forming right after depletion of reactants, occurrence of which was reproduced in three experiments. This transient phase was short-lived, exhibiting low-intensity Bragg reflections, most notably at $d = 12.33$ Å (corresponding to 0.82° in 2Θ for radiation wavelength $\lambda = 0.177$ Å) and 7.51 Å (1.35° in 2Θ) (Figure S6). Unfortunately, since its presence in the reaction mixture lasted, on average, less than 60 s, we were not able to isolate it or identify it on the basis of the *in situ* collected patterns. We could not identify this intermediate also in *in situ* Raman spectra. Rietveld analysis was here hamstrung not only by the appearance of a crystallographically unidentified intermediate, but also by impurities originating from the starting NaI. While the resulting reaction mixture was predominately composed of AgI and $NaNO_3$, we were unable to assign a phase to the Bragg reflection with $d = 3.97$ Å(2.55° in 2Θ) (Figures 4a, S7 and S8).

We were intrigued by the formation of Ag_2ClNO_3 as an intermediate since its analogs with bromide and iodide, Ag_2BrNO_3 and Ag_2INO_3, were not observed during mechanochemical metathesis. Considering that milling reactions were often found to follow the Ostwald's rule of stages,[94,95] where intermediate phases occur starting from a higher-energy content phase which is then transforming into phases of increasingly lower energy content, we have assumed that only Ag_2ClNO_3 would have a lower energy than the mixture of AgX and $AgNO_3$. Since the bromide and iodide analogs are known in the literature, we were interested in preparing Ag_2BrNO_3 and Ag_2INO_3 mechanochemically. Previous reports of their preparation describe a solvent-based synthesis at an elevated temperature.[89,104,105] Here, milling of AgX (X = Cl, Br, or I) with $AgNO_3$ at room temperature for 70 minutes yielded all three Ag_2XNO_3

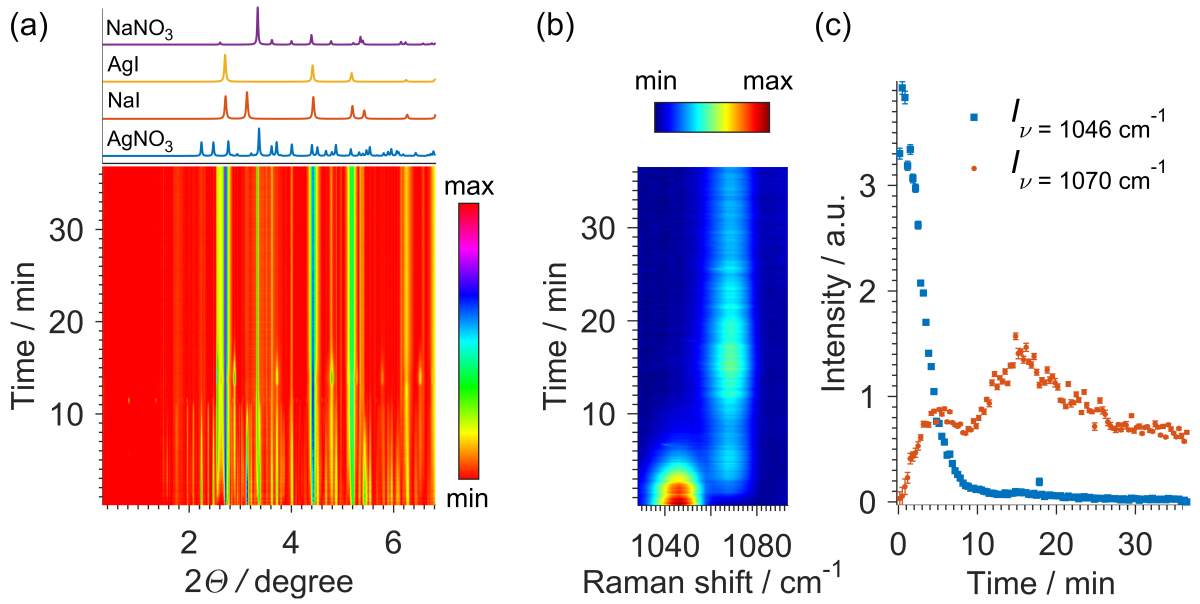

Figure 4: Milling of $AgNO_3$ and NaI. (a) *in situ* reaction monitoring by synchrotron PXRD. Diffraction patterns of reactants and products are given above the 2D time-resolved spectra. (b) 2D time-resolved Raman spectra for the Raman spectral range $1088 - 1030\,cm^{-1}$. (c) The change of Raman peak intensities at 1046 and $1070\,cm^{-1}$ during milling. There was an sharp increase in intensities of Raman band at $1070\,cm^{-1}$ that are more likely due to the sticking of the reaction mixture. These changes correlated with the sharp increase of Bragg reflections in PXRD patterns, typically observed in cases of inhomogeneous distribution of the reaction mixture during milling.[55]

pure double salts, as evidenced by Rietveld analysis of their PXRD patterns collected *ex situ* (Figure S9–S11).

Since standard enthalpies and Gibbs energies of formation of these double salts are not known in the literature, we have estimated them using solid-state density functional theory (DFT) calculations (Figure 5). Assuming a reaction path with intermediate formation of the Ag_2XNO_3, we find that all three double salts should have formed, according to the Ostwald's rule of stages. A likely reason why we did not observe formation of Ag_2BrNO_3 and Ag_2INO_3 *in situ* lies in kinetics – $AgNO_3$ is potentially faster to react with NaX than with the nascent AgX. While results of our calculations are in good agreement with the experimental reaction enthalpies (Table 1) one should bear in mind that these calculations assume temperature of 0 K and yield no entropy contribution, and thus cannot calculate Gibbs energies. However, the reaction rates in the NaX series seem to correlate with reaction enthalpies.

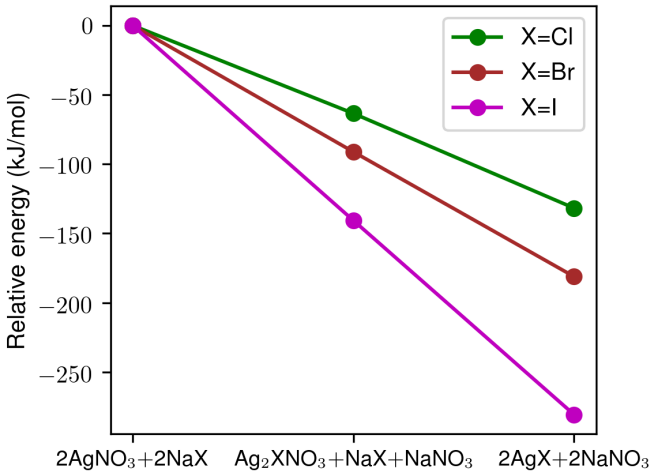

Figure 5: DFT-estimated relative energies of the reaction mixture taking the transformation path via the intermediate double salt Ag_2XNO_3. Energies of the starting and final compositions need to be divided by 2 for comparison with values in Table 1.

Finally, we noticed that some samples had changed color and became slightly purplish of greyish after milling. This was likely due to partial silver reduction, but since we minimised exposure to light during milling, we assumed that high-energy ball impacts may have led to localised high temperatures causing a disproportionation reaction of AgCl with the formation

of elementary Ag(0) and Cl_2. To test this assumption, in a repeated experiment, atmosphere inside the milling vessel was analysed by mass spectrometry after 60 min milling to reveal a slight increase in the partial pressure of Cl_2 (Figure S12). Our mass spectrometer was limited to detection of ions with relative mass below 100 so only the experiment with NaCl was feasible to be analysed in this way by mass spectrometry. Noteworthy, we did not observe an increase in the amount of any N_xO_y species after milling that could have resulted from decomposition of the nitrate ion, indicating that the potential hot spots during milling did not generate conditions that could lead to nitrate decomposition. We are currently developing a setup which would allow for an *in situ* measurement of gaseous products during milling, in a manner similar to the one recently described.[106]

Conclusion

In situ monitoring was applied to a ball-milling metathesis reaction between $AgNO_3$ and NaX (X = Cl, Br, or I). Reactions, conducted by neat grinding of solids, resulted in the formation of the expected products, AgX and $NaNO_3$. Reaction rates for milling of $AgNO_3$ with NaI and NaBr were similar and significantly faster then the reaction rate with NaCl. A slower reaction for NaCl was possibly a consequence of the formation of the intermediate Ag_2ClNO_3, while the corresponding intermediates did not form with NaBr and NaI. All three double salts could have been expected as intermediates based on the Ostwald's rule of stages and moreover, can be efficiently prepared by milling of AgX and $AgNO_3$. In addition, we find it interesting that the nascent $NaNO_3$ has crystallised as the unstable disordered polymorph before it transformed into the room-temperature-stable ordered one, and we intend to investigate this further. We have thus demonstrated that a metathesis reaction between ionic compounds can be performed efficiently at ambient conditions by ball milling of solids, and that such reaction may exhibit reactive intermediates, much as reactions of organic or metal-organic systems. We also present an efficient and elegant means for the

preparation of double salts without any post-synthetic work-up required. Having succesfully applied *in situ* reaction monitoring to mechanochemical reactions between inorganic ionic compounds, we have completed application of these techniques to mechanochemical reactions of all major classes of compounds.

Acknowledgement

We thank to Dr Krunoslav Užarević and Dr Martina Tireli for assistance and discussion. We are grateful to the Ruđer Bošković Institute for financial support and to the ESRF for beamtime. SL is supported by the Croatian Science foundation. This work was supported by the COST Action CA18112 - Mechanochemistry for Sustainable Industry and in part by the Croatian Science Foundation (grant No. 4744). IL acknowledge support from the European Union through the European Regional Development Fund within the Competitiveness and Cohesion Operational Programme (Grant No. KK.01.1.1.06).

Supporting Information Available

Supporting information contains table of standard reaction enthalpies, entropies, and Gibbs energies, *ex situ* laboratory PXRD patterns, as well as *in situ* Raman spectra, and Rietveld refinement plots.

This material is available free of charge via the Internet at `http://pubs.acs.org/`.

References

(1) Do, J.-L.; Friščić, T. Mechanochemistry: A Force of Synthesis. *ACS Cent. Sci.* **2017**, *3*, 13–19.

(2) Howard, J.; Cao, Q.; Browne, D. L. Mechanochemistry as an emerging tool for molecular synthesis: what can it offer? *Chem. Sci.* **2018**, *9*, 3080–3094.

(3) Do, J.-L.; Friščić, T. Chemistry 2.0: Developing a New, Solvent-Free System of Chemical Synthesis Based on Mechanochemistry. *Synlett* **2017**, *28*, 2066–2092, 2066.

(4) Tan, D.; García, F. Main group mechanochemistry: from curiosity to established protocols. *Chem. Soc. Rev.* **2019**, *48*, 2274–2292.

(5) Hernández, J. G.; Bolm, C. Altering Product Selectivity by Mechanochemistry. *J. Org. Chem.* **2017**, *82*, 4007–4019.

(6) Friščić, T.; Mottillo, C.; Titi, H. M. Mechanochemistry for Synthesis. *Angew. Chem. Int. Ed.* **2020**, *59*, 1018–1029.

(7) Andersen, J.; Mack, J. Mechanochemistry and organic synthesis: from mystical to practical. *Green Chem.* **2018**, *20*, 1435–1443.

(8) Tan, D.; Friščić, T. Mechanochemistry for Organic Chemists: An Update. *Eur. J. Org. Chem.* **2018**, *2018*, 18–33.

(9) Wang, G.-W. Mechanochemical organic synthesis. *Chem. Soc. Rev.* **2013**, *42*, 7668–7700.

(10) Egorov, I. N.; Santra, S.; Kopchuk, D. S.; Kovalev, I. S.; Zyryanov, G. V.; Majee, A.; Ranu, B. C.; Rusinov, V. L.; Chupakhin, O. N. Ball milling: an efficient and green approach for asymmetric organic syntheses. *Green Chem.* **2020**, –.

(11) Šepelák, V.; Düvel, A.; Wilkening, M.; Becker, K.-D.; Heitjans, P. Mechanochemical reactions and syntheses of oxides. *Chem. Soc. Rev.* **2013**, *42*, 7507–7520.

(12) Boldyreva, E. Mechanochemistry of inorganic and organic systems: what is similar, what is different? *Chem. Soc. Rev.* **2013**, *42*, 7719–7738.

(13) Šepelák, V.; Bégin-Colin, S.; Le Caër, G. Transformations in oxides induced by high-energy ball-milling. *Dalton Trans.* **2012**, *41*, 11927–11948.

(14) Xu, C.; De, S.; Balu, A. M.; Ojeda, M.; Luque, R. Mechanochemical synthesis of advanced nanomaterials for catalytic applications. *Chem. Commun.* **2015**, *51*, 6698–6713.

(15) Beillard, A.; Bantreil, X.; Métro, T.-X.; Martinez, J.; Lamaty, F. Alternative Technologies That Facilitate Access to Discrete Metal Complexes. *Chem. Rev.* **2019**, *119*, 7529–7609.

(16) Koby, R. F.; Hanusa, T. P.; Schley, N. D. Mechanochemically Driven Transformations in Organotin Chemistry: Stereochemical Rearrangement, Redox Behavior, and Dispersion-Stabilized Complexes. *J. Am. Chem. Soc.* **2018**, *140*, 15934–15942.

(17) Rightmire, N. R.; Hanusa, T. P. Advances in organometallic synthesis with mechanochemical methods. *Dalton Trans.* **2016**, *45*, 2352–2362.

(18) Beillard, A.; Métro, T.-X.; Bantreil, X.; Martinez, J.; Lamaty, F. Cu(0), O_2 and mechanical forces: a saving combination for efficient production of Cu-NHC complexes. *Chem. Sci.* **2017**, *8*, 1086–1089.

(19) Bjelopetrović, A.; Lukin, S.; Halasz, I.; Užarević, K.; Đilović, I.; Barišić, D.; Budimir, A.; Juribašić Kulcsár, M.; Ćurić, M. Mechanism of Mechanochemical C-H Bond Activation in an Azobenzene Substrate by Pd(II) Catalysts. *Chem. Eur. J.* **2018**, *24*, 10672–10682.

(20) Friščić, T. Supramolecular concepts and new techniques in mechanochemistry: cocrystals, cages, rotaxanes, open metal-organic frameworks. *Chem. Soc. Rev.* **2012**, *41*, 3493–3510.

(21) Delori, A.; Friščić, T.; Jones, W. The role of mechanochemistry and supramolecular design in the development of pharmaceutical materials. *CrystEngComm* **2012**, *14*, 2350–2362.

(22) Hasa, D.; Schneider Rauber, G.; Voinovich, D.; Jones, W. Cocrystal Formation through Mechanochemistry: from Neat and Liquid-Assisted Grinding to Polymer-Assisted Grinding. *Angew. Chem. Int. Ed.* **2015**, *54*, 7371–7375.

(23) Friščić, T.; Jones, W. Recent Advances in Understanding the Mechanism of Cocrystal Formation via Grinding. *Cryst. Growth Des.* **2009**, *9*, 1621–1637.

(24) Baláž, P.; Achimovičová, M.; Baláž, M.; Billik, P.; Cherkezova-Zheleva, Z.; Criado, J. M.; Delogu, F.; Dutková, E.; Gaffet, E.; Gotor, F. J.; Kumar, R.; Mitov, I.; Rojac, T.; Senna, M.; Streletskii, A.; Wieczorek-Ciurowa, K. Hallmarks of mechanochemistry: from nanoparticles to technology. *Chem. Soc. Rev.* **2013**, *42*, 7571–7637.

(25) James, S. L.; Adams, C. J.; Bolm, C.; Braga, D.; Collier, P.; Friščić, T.; Grepioni, F.; Harris, K. D. M.; Hyett, G.; Jones, W.; Krebs, A.; Mack, J.; Maini, L.; Orpen, A. G.; Parkin, I. P.; Shearouse, W. C.; Steed, J. W.; Waddell, D. C. Mechanochemistry: opportunities for new and cleaner synthesis. *Chem. Soc. Rev.* **2012**, *41*, 413–447.

(26) Chen, D.; Zhao, J.; Zhang, P.; Dai, S. Mechanochemical synthesis of metal-organic frameworks. *Polyhedron* **2019**, *162*, 59–64.

(27) Pichon, A.; Lazuen-Garay, A.; James, S. L. Solvent-free synthesis of a microporous metal-organic framework. *CrystEngComm* **2006**, *8*, 211–214.

(28) Friščiś, T.; Halasz, I.; Štrukil, V.; Eckert-Maksiś, M.; Dinnebier, R. Clean and efficient synthesis using mechanochemistry: Coordination polymers, metal-organic frameworks and metallodrugs. *Croat. Chem. Acta* **2012**, *85*, 367–378.

(29) Stolar, T.; Užarević, K. Mechanochemistry: an efficient and versatile toolbox for synthesis, transformation, and functionalization of porous metal-organic frameworks. *CrystEngComm* **2020**, –.

(30) Shi, Y. X.; Xu, K.; Clegg, J. K.; Ganguly, R.; Hirao, H.; Friščić, T.; Garcìa, F. The First Synthesis of the Sterically Encumbered Adamantoid Phosphazane $P_4(NtBu)_6$: Enabled by Mechanochemistry. *Angew. Chem. Int. Ed.* **2016**, *55*, 12736–12740.

(31) Sim, Y.; Shi, Y. X.; Ganguly, R.; Li, Y.; Garcìa, F. Mechanochemical Synthesis of Phosphazane-Based Frameworks. *Chem. Eur. J.* **2017**, *23*, 11279–11285.

(32) Sim, Y.; Tan, D.; Ganguly, R.; Li, Y.; Garcìa, F. Orthogonality in main group compounds: a direct one-step synthesis of air- and moisture-stable cyclophosphazanes by mechanochemistry. *Chem. Commun.* **2018**, *54*, 6800–6803.

(33) Speight, I. R.; Chmely, S. C.; Hanusa, T. P.; Rheingold, A. L. Mechanochemically directed metathesis in group 2 chemistry: calcium amide formation without solvent. *Chem. Commun.* **2019**, *55*, 2202–2205.

(34) Ardila-Fierro, K. J.; Crawford, D. E.; Körner, A.; James, S. L.; Bolm, C.; Hernández, J. G. Papain-catalysed mechanochemical synthesis of oligopeptides by milling and twin-screw extrusion: application in the Juliá-Colonna enantioselective epoxidation. *Green Chem.* **2018**, *20*, 1262–1269.

(35) Cheng, H.; Hernández, J. G.; Bolm, C. Mechanochemical Ruthenium-Catalyzed Hydroarylations of Alkynes under Ball-Milling Conditions. *Org. Lett.* **2017**, *19*, 6284–6287.

(36) Cheng, H.; Hernández, J. G.; Bolm, C. Mechanochemical Cobalt-Catalyzed CâĹŠH Bond Functionalizations by Ball Milling. *Adv. Synth. Catal.* **2018**, *360*, 1800–1804.

(37) Hernández, J. G.; Ardila-Fierro, K. J.; Crawford, D.; James, S. L.; Bolm, C. Mechanoenzymatic peptide and amide bond formation. *Green Chem.* **2017**, *19*, 2620–2625.

(38) Nicholson, W. I.; Seastram, A. C.; Iqbal, S. A.; Reed-Berendt, B. G.; Morrill, L. C.;

Browne, D. L. N-Heterocyclic Carbene Acyl Anion Organocatalysis by Ball-Milling. *ChemSusChem* **2020**, *13*, 131–135.

(39) Vogt, C. G.; Grätz, S.; Lukin, S.; Halasz, I.; Etter, M.; Evans, J. D.; Borchardt, L. Direct Mechanocatalysis: Palladium as Milling Media and Catalyst in the Mechanochemical Suzuki Polymerization. *Angew. Chem. Int. Ed.* **2019**, *58*, 18942–18947.

(40) Porcheddu, A.; Colacino, E.; De Luca, L.; Delogu, F. Metal-Mediated and Metal-Catalyzed Reactions Under Mechanochemical Conditions. *ACS Catal.* **2020**,

(41) Cocco, G.; Delogu, F.; Schiffini, L. Toward a Quantitative Understanding of the Mechanical Alloying Process. *J. Mater. Synth. Process.* **2000**, *8*, 167–180.

(42) Delogu, F.; Takacs, L. Information on the mechanism of mechanochemical reaction from detailed studies of the reaction kinetics. *J. Mater. Sci.* **2018**, *53*, 13331–13342.

(43) Garroni, S.; Delogu, F.; Bonatto Minella, C.; Pistidda, C.; Cuesta-Lopez, S. Mechanically activated metathesis reaction in $NaNH_2$-MgH_2 powder mixtures. *J. Mater. Sci.* **2017**, *52*, 11891–11899.

(44) Ma, X.; Yuan, W.; Bell, S. E. J.; James, S. L. Better understanding of mechanochemical reactions: Raman monitoring reveals surprisingly simple pseudo-fluid model for a ball milling reaction. *Chem. Commun.* **2014**, *50*, 1585–1587.

(45) Tumanov, I. A.; Achkasov, A. F.; Boldyreva, E. V.; Boldyrev, V. V. About the possibilities to detect intermediate stages in mechanochemical synthesis of molecular complexes. *Russ. J. Phys. Chem. A* **2012**, *86*, 1014–1017.

(46) Strobridge, F. C.; Judaš, N.; Friščić, T. A stepwise mechanism and the role of water in the liquid-assisted grinding synthesis of metal-organic materials. *CrystEngComm* **2010**, *12*, 2409–2418.

(47) Tröbs, L.; Emmerling, F. Mechanochemical synthesis and characterisation of cocrystals and metal organic compounds. *Faraday Discuss.* **2014**, *170*, 109–119.

(48) Pisk, J.; Hrenar, T.; Rubčić, M.; Pavlović, G.; Damjanović, V.; Lovrić, J.; Cindrić, M.; Vrdoljak, V. Comparative studies on conventional and solvent-free synthesis toward hydrazones: application of PXRD and chemometric data analysis in mechanochemical reaction monitoring. *CrystEngComm* **2018**, *20*, 1804–1817.

(49) Užarević, K.; Ferdelji, N.; Mrla, T.; Julien, P. A.; Halasz, B.; Friščić, T.; Halasz, I. Enthalpy vs. friction: heat flow modelling of unexpected temperature profiles in mechanochemistry of metal-organic frameworks. *Chem. Sci.* **2018**, *9*, 2525–2532.

(50) Cliffe, M. J.; Mottillo, C.; Stein, R. S.; Bučar, D.-K.; Friščić, T. Accelerated aging: a low energy, solvent-free alternative to solvothermal and mechanochemical synthesis of metal-organic materials. *Chem. Sci.* **2012**, *3*, 2495–2500.

(51) Hammerer, F.; Loots, L.; Do, J.-L.; Therien, J. P. D.; Nickels, C. W.; Friščić, T.; Auclair, K. Solvent-Free Enzyme Activity: Quick, High-Yielding Mechanoenzymatic Hydrolysis of Cellulose into Glucose. *Angew. Chem. Int. Ed.* **2018**, *57*, 2621–2624.

(52) Di Nardo, T.; Hadad, C.; Nguyen Van Nhien, A.; Moores, A. Synthesis of high molecular weight chitosan from chitin by mechanochemistry and aging. *Green Chem.* **2019**, *21*, 3276–3285.

(53) Riss-Yaw, B.; Métro, T.-X.; Lamaty, F.; Coutrot, F. Association of liquid-assisted grinding with aging accelerates the inherently slow slipping-on of a dibenzo-24-crown-8 over the N-hydroxysuccinimide ester of an ammonium-containing thread. *RSC Adv.* **2019**, *9*, 21587–21590.

(54) Užarević, K.; Halasz, I.; Friščić, T. Real-Time and In Situ Monitoring of Mechanochemical Reactions: A New Playground for All Chemists. *J. Phys. Chem. Lett.* **2015**, *6*, 4129–4140.

(55) Friščić, T.; Halasz, I.; Beldon, P. A.; Belenguer, A. M.; Adams, F.; Kimber, S. A. J.; Honkimäki, V.; Dinnebier, R. E. Real-time and in situ monitoring of mechanochemical milling reactions. *Nature Chem.* **2013**, *5*, 66–73.

(56) Halasz, I.; Kimber, S. A. J.; Beldon, P. J.; Belenguer, A. M.; Adams, F.; Honkimäki, V.; Nightingale, R. C.; Dinnebier, R. E.; Friščić, T. In situ and real-time monitoring of mechanochemical milling reactions using synchrotron X-ray diffraction. *Nat. Protoc.* **2013**, *8*, 1718–1729.

(57) Katsenis, A. D.; A., P.; Štrukil, V.; Mottillo, C.; Julien, P. A.; Užarević, M. H., K. Pham; Do, T. O.; Kimber, S. A. J.; Lazić, P.; Magdysyuk, O.; Dinnebier, R. E.; Halasz, I.; Friščić, T. In situ X-ray diffraction monitoring of a mechanochemical reaction reveals a unique topology metal-organic framework. *Nat. Commun.* **2015**, *6*, 6662.

(58) Ban, V.; Sadikin, Y.; Lange, M.; Tumanov, N.; Filinchuk, Y.; Černý, R.; Casati, N. Innovative in Situ Ball Mill for X-ray Diffraction. *Anal. Chem.* **2017**, *89*, 13176–13181.

(59) Gracin, D.; Štrukil, V.; Friščić, T.; Halasz, I.; Užarević, K. Laboratory Real-Time and In Situ Monitoring of Mechanochemical Milling Reactions by Raman Spectroscopy. *Angew. Chem. Int. Ed.* **2014**, *53*, 6193–6197.

(60) Julien, P. A.; Malvestiti, I.; Friščić, T. The effect of milling frequency on a mechanochemical organic reaction monitored by in situ Raman spectroscopy. *Beilstein J. Org. Chem.* **2017**, *13*, 2160–2168.

(61) Tireli, M.; Juribašić Kulcsar, M.; Cindro, N.; Gracin, D.; Biliškov, N.; Borovina, M.; Ćurić, M.; Halasz, I.; Užarević, K. Mechanochemical reactions studied by in situ Raman spectroscopy: base catalysis in liquid-assisted grinding. *Chem. Commun.* **2015**, *51*, 8058–8061.

(62) Juribašić, M.; Užarević, K.; Gracin, D.; Ćurić, M. Mechanochemical C-H bond activation: rapid and regioselective double cyclopalladation monitored by in situ Raman spectroscopy. *Chem. Commun.* **2014**, *50*, 10287–10290.

(63) Fischer, F.; Fendel, N.; Greiser, S.; Rademann, K.; Emmerling, F. Impact Is Important - Systematic Investigation of the Influence of Milling Balls in Mechanochemical Reactions. *Org. Process Res. Dev.* **2017**, *21*, 655–659.

(64) Užarević, K.; Štrukil, V.; Mottillo, C.; Julien, P. A.; Puškarić, A.; Friščić, T.; Halasz, I. Exploring the Effect of Temperature on a Mechanochemical Reaction by in Situ Synchrotron Powder X-ray Diffraction. *Cryst. Growth Des.* **2016**, *16*, 2342–2347.

(65) Doppiu, S.; Schultz, L.; Gutfleisch, O. In situ pressure and temperature monitoring during the conversion of Mg into MgH_2 by high-pressure reactive ball milling. *J. Alloys Compd* **2007**, *427*, 204 – 208.

(66) Brekalo, I.; Yuan, W.; Mottillo, C.; Lu, Y.; Zhang, Y.; Casaban, J.; Holman, K. T.; James, S. L.; Duarte, F.; Williams, P. A.; Harris, K. D. M.; Friščić, T. Manometric real-time studies of the mechanochemical synthesis of zeolitic imidazolate frameworks. *Chem. Sci.* **2020**, *11*, 2141–2147.

(67) van Bonn, P.; Bolm, C.; Hernández, J. G. Mechanochemical Palladium-Catalyzed Carbonylative Reactions Using $Mo(CO)_6$. *Chem. Eur. J.* **2020**, *26*, 2576–2580.

(68) Lukin, S.; Stolar, T.; Tireli, M.; Blanco, M. V.; Babić, D.; Friščić, T.; Užarević, K.; Halasz, I. Tandem In Situ Monitoring for Quantitative Assessment of Mechanochemical Reactions Involving Structurally Unknown Phases. *Chem. Eur. J.* **2017**, *23*, 13941–13949.

(69) Lukin, S.; Tireli, M.; Stolar, T.; Barišić, D.; Blanco, M. V.; di Michiel, M.; Užarević, K.; Halasz, I. Isotope Labeling Reveals Fast Atomic and Molecular Exchange in Mechanochemical Milling Reactions. *J. Am. Chem. Soc.* **2019**, *141*, 1212–1216.

(70) Batzdorf, L.; Fischer, F.; Wilke, M.; Wenzel, K.-J.; Emmerling, F. Direct In Situ Investigation of Milling Reactions Using Combined X-ray Diffraction and Raman Spectroscopy. *Angew. Chem. Int. Ed.* **2015**, *54*, 1799–1802.

(71) Kulla, H.; Wilke, M.; Fischer, F.; Röllig, M.; Maierhofer, C.; Emmerling, F. Warming up for mechanosynthesis – temperature development in ball mills during synthesis. *Chem. Commun.* **2017**, *53*, 1664–1667.

(72) Lukin, S.; Lončarić, I.; Tireli, M.; Stolar, T.; Blanco, M. V.; Lazić, P.; Užarević, K.; Halasz, I. Experimental and Theoretical Study of Selectivity in Mechanochemical Cocrystallization of Nicotinamide with Anthranilic and Salicylic Acid. *Cryst. Growth Des.* **2018**, *18*, 1539–1547.

(73) Fischer, F.; Greiser, S.; Pfeifer, D.; Jäger, C.; Rademann, K.; Emmerling, F. Mechanochemically Induced Conversion of Crystalline Benzamide Polymorphs by Seeding. *Angew. Chem. Int. Ed.* **2016**, *55*, 14281–14285.

(74) Kulla, H.; Greiser, S.; Benemann, S.; Rademann, K.; Emmerling, F. Knowing When To Stop–Trapping Metastable Polymorphs in Mechanochemical Reactions. *Cryst. Growth Des.* **2017**, *17*, 1190–1196.

(75) Kulla, H.; Michalchuk, A. A. L.; Emmerling, F. Manipulating the dynamics of mechanochemical ternary cocrystal formation. *Chem. Commun.* **2019**, *55*, 9793–9796.

(76) Surov, A. O.; Vasilev, N. A.; Churakov, A. V.; Stroh, J.; Emmerling, F.; Perlovich, G. L. Solid Forms of Ciprofloxacin Salicylate: Polymorphism, Formation Pathways, and Thermodynamic Stability. *Cryst. Growth Des.* **2019**, *19*, 2979–2990.

(77) Akhmetova, I.; Schutjajew, K.; Wilke, M.; Buzanich, A.; Rademann, K.; Roth, C.; Emmerling, F. Synthesis, characterization and in situ monitoring of the mechanochemical reaction process of two manganese(II)-phosphonates with N-containing ligands. *J. Mater. Sci.* **2018**, *53*, 13390–13399.

(78) Lukin, S.; Tireli, M.; Lončarić, I.; Barišić, D.; Šket, P.; Vrsaljko, D.; di Michiel, M.; Plavec, J.; Užarević, K.; Halasz, I. Mechanochemical carbon–carbon bond formation that proceeds via a cocrystal intermediate. *Chem. Commun.* **2018**, *54*, 13216–13219.

(79) Boldyrev, V. V.; Avvakumov, E. G. Mechanochemistry of Inorganic Solids. *Russ. Chem. Rev.* **1971**, *40*, 847–859.

(80) Takacs, L. What is unique about mechanochemical reactions? *Acta Phys. Pol. A* **2014**, *126*, 1040–1043.

(81) Colacino, E.; Carta, M.; Pia, G.; Porcheddu, A.; Ricci, P. C.; Delogu, F. Processing and Investigation Methods in Mechanochemical Kinetics. *ACS Omega* **2018**, *3*, 9196–9209.

(82) Eilers, P. H. C.; Boelens, H. F. M. Baseline correction with Asymmetric Least Squares Smoothing. *Leiden University Medical Center Report* **2005**,

(83) Kresse, G.; Furthmüller, J. Efficient iterative schemes for ab initio total-energy calculations using a plane-wave basis set. *Phys. Rev. B* **1996**, *54*, 11169–11186.

(84) Kresse, G.; Furthmüller, J. Efficiency of ab-initio total energy calculations for metals and semiconductors using a plane-wave basis set. *Comput. Mater. Sci.* **1996**, *6*, 15–50.

(85) Perdew, J. P.; Burke, K.; Ernzerhof, M. Generalized Gradient Approximation Made Simple. *Phys. Rev. Lett.* **1996**, *77*, 3865–3868.

(86) Blöchl, P. E. Projector augmented-wave method. *Phys. Rev. B* **1994**, *50*, 17953–17979.

(87) Monkhorst, H. J.; Pack, J. D. Special points for Brillouin-zone integrations. *Phys. Rev. B* **1976**, *13*, 5188–5192.

(88) CRC Handbook, *CRC Handbook of Chemistry and Physics, 97th Edition*, 97th ed.; CRC Press, 2017.

(89) Persson, K. Structure of disilver chloride nitrate. *Acta Cryst. B* **1979**, *35*, 1432–1435.

(90) Paul, G. L.; Pryor, A. W. The study of sodium nitrate by neutron diffraction. *Acta Cryst. B* **1972**, *28*, 2700–2702.

(91) D'Aguanno, B.; Karthik, M.; Grace, A.; Floris, A. Thermostatic properties of nitrate molten salts and their solar and eutectic mixtures. *Sci. Rep.* **2018**, *8*.

(92) Cherin, P.; Hamilton, W. C.; Post, B. Position and thermal parameters of oxygen atoms in sodium nitrate. *Acta Cryst.* **1967**, *23*, 455–460.

(93) Harris, M. A new explanation for the unusual critical behavior of calcite and sodium nitrate, NaNO3. *Am. Mineral.* **1999**, *84*, 1632 – 1640.

(94) Burley, J. C.; Duer, M. J.; Stein, R. S.; Vrcelj, R. M. Enforcing Ostwald's rule of stages: Isolation of paracetamol forms III and II. *Eur. J. Pharm. Sci.* **2007**, *31*, 271 – 276.

(95) Akimbekov, Z.; Katsenis, A. D.; Nagabhushana, G. P.; Ayoub, G.; Arhangelskis, M.; Morris, A. J.; Friščić, T.; Navrotsky, A. Experimental and Theoretical Evaluation of the Stability of True MOF Polymorphs Explains Their Mechanochemical Interconversions. *J. Am. Chem. Soc.* **2017**, *139*, 7952–7957.

(96) Požar, J. University of Zagreb, personal communication.

(97) Cao, S.; Bennett, T. D.; Keen, D. A.; Goodwin, A. L.; Cheetham, A. K. Amorphization of the prototypical zeolitic imidazolate framework ZIF-8 by ball-milling. *Chem. Commun.* **2012**, *48*, 7805–7807.

(98) Delogu, F.; Cocco, G. Kinetics of amorphization processes by mechanical alloying: A modeling approach. *J. Alloys Compd.* **2007**, *436*, 233–240.

(99) Chen, Y.; Bibole, M.; Le Hazif, R.; Martin, G. Ball-milling-induced amorphization in Ni_xZr_y compounds: A parametric study. *Phys. Rev. B* **1993**, *48*, 14–21.

(100) Dujardin, N.; Willart, J. F.; Dudognon, E.; Danède, F.; Descamps, M. Mechanism of Solid State Amorphization of Glucose upon Milling. *J. Phys. Chem. B* **2013**, *117*, 1437–1443.

(101) Caron, V.; Willart, J.-F.; Lefort, R.; Derollez, P.; Danede, F.; Descamps, M. Solid state amorphization kinetic of alpha lactose upon mechanical milling. *Carbohydr. Res.* **2011**, *346*, 2622–2628.

(102) Xu, K.; Chen, Y. Raman spectroscopic studies of mixed crystals of $NaNO_3$–KNO_3 quenched from different temperatures: evidence for limited solid solutions in the system. *J. Raman Spectrosc.* **1999**, *30*, 441–448.

(103) Shen, Z. X.; Sherman, W. F.; Kuok, M. H.; Tang, S. H. IR and Raman spectra of $AgNO_3$ at low temperatures. *J. Raman Spectrosc.* **1992**, *23*, 509–514.

(104) Persson, K. The crystal structure of Ag_2INO_3. *Acta Cryst. B* **1979**, *35*, 302–306.

(105) Persson, K.; Holmberg, B. The crystal structure of Ag_2BrNO_3. *Acta Cryst. B* **1977**, *33*, 3768–3772.

(106) Tricker, A. W.; Samaras, G.; Hebisch, K. L.; Realff, M. J.; Sievers, C. Hot spot generation, reactivity, and decay in mechanochemical reactors. *Chem. Eng. J.* **2020**, *382*, 122954.

Graphical TOC Entry

In situ reaction monitoring of mechanochemistry of simple ionic salts provides the first insight into archetypal ionic exchange reactions to reveal complex and diverse reaction mechanisms.